CZTS absorber layer for thin film solar cells from electrodeposited metallic stacked precursors (Zn/Cu-Sn)

M.I. Khalil [a], O. Atici [a], A. Lucotti [b], S. Binetti [c], A. Le Donne [c], L. Magagnin [a,*]

[a] Dipartimento di Chimica, Materiali e Ing. Chimica "Giulio Natta", Politecnico di Milano, Via Mancinelli 7, 20131 Milano, Italy
[b] Dipartimento di Chimica, Materiali e Ing. Chimica "Giulio Natta", Politecnico di Milano, Piazza Leonardo da Vinci 32, 20133 Milano, Italy
[c] Department of Materials Science and Solar Energy Research Centre (MIB-SOLAR), University of Milano- Bicocca, Via Cozzi 53, 20125 Milano, Italy

In the present work, Kesterite-Cu2ZnSnS4 (CZTS) thin films were successfully synthesized from stacked bilayer precursor (Zn/Cu-Sn) through electrodeposition-annealing route. Adherent and homogeneous Cu-poor, Zn-rich stacked metal Cu-Zn-Sn precursors with different compositions were sequentially elec-trodeposited, in the order of Zn/Cu-Sn onto Mo foil substrates. Subsequently, stacked layers were soft annealed at 350 ◦C for 20 min in flowing N2 atmosphere in order to improve intermixing of the elements. Then, sulfurization was completed at 585 ◦C for 15 min in elemental sulfur environment in a quartz tube furnace with N2 atmosphere. Morphological, compositional and structural properties of the films were investigated using SEM, EDS and XRD methods. Raman spectroscopy with two different excitation lines (514.5 and 785 nm), has been carried out on the sulfurized films in order to fully characterize the CZTS phase. Higher excitation wavelength showed more secondary phases, but with low intensities. Glow dis-charge optical emission spectroscopy (GDOES) has also been performed on films showing well formed Kesterite CZTS along the film thickness as compositions of the elements do not change along the thick-ness. In order to investigate the electronic structure of the CZTS, Photoluminescence (PL) spectroscopy has been carried out on the films, whose results matched up with the literatures.

Keywords Kesterite, CZTS, Bilayer precursor, Sulfurization, Photoluminescence etc

1. Introduction

Thin film solar cells have been attracted steady by many researchers during last 20 years and considered as an alternative technology to Si-based solar cells due to their low cost and almost compatible conversion efficiencies. Market share of thin film PV solar cells are around 10% where CdTe and $CuIn(Ga)(Se)_2$ (CIGS) are dominant as absorber layers [1]. However, In, Ga and Te are not earth abundant, while on the other hand Cd and Se are both toxic elements. Alternatively, Cu_2ZnSnS_4 (CZTS) is a promising material due to the fact that Zn and Sn are cheap, non-toxic and earth abundant elements. Furthermore, CZTS is a *p*-type semiconductor with direct bandgap energy close to 1.5 eV and a large absorption coefficient over $10^4\ cm^{-1}$ as well as theoretical conversion efficiency of 32.2% which make it suitable among all the thin film solar cells [2,3].

Article history:
Received 25 September 2015
Received in revised form 7 April 2016
Accepted 10 April 2016
Available online 11 April 2016

Several methods have been used to prepare CZTS thin films such as sputtering, evaporation, spray pyrolysis, solution-based methods, electrodeposition method, etc. The highest conversion efficiency was achieved for sulfo-selenide thin films (CZTSSe) ($\eta = 12.6\%$) by Wang et al. using hydrazine-based solution process [4]. However, in case of pure sulfide CZTS thin films, highest 9.2% power conversion efficiency was demonstrated by Kato et al. by using evaporation-annealing route [5]. Among different deposition techniques, electrodeposition is one of the promising methods for preparing CZTS absorber films because of its low cost equipment's, large scale production and good control over the composition and morphology. Generally, electrodeposition-based process can be divided into two categories. The former is two-steps process where electrodeposition of Cu-Zn-Sn metal precursors is followed by a sulfurization process. The latter is single-step co-electrodeposition of Cu, Zn, Sn and S directly to form CZTS compound. However, it is very difficult to deposit homogenous and good crystalline CZTS films from single-step electrodeposition process due to the large reduction potential window among the elements. Electrodeposition of Cu-Zn-Sn can be done in two ways; (i) simultaneous electrodeposition of Cu-Zn-Sn from single electrolyte and (ii) sequential electrodeposition of Cu-Zn-Sn from different electrolytes with var-

* Corresponding author.
E-mail addresses: mdibrahim.khalil@polimi.it (M.I. Khalil), luca.magagnin@polimi.it (L. Magagnin).

Published Journal Article available at: http://dx.doi.org/10.1016/j.apsusc.2016.04.062

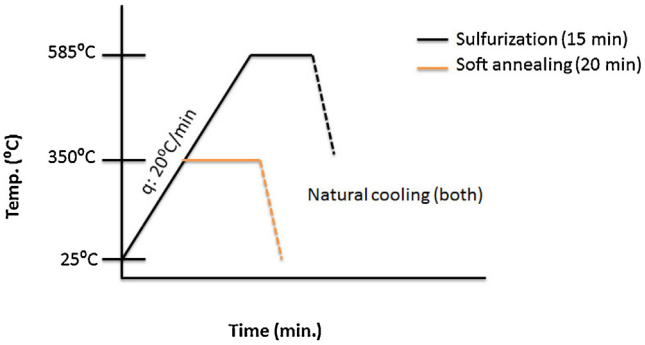

Fig. 1. Schematic temperature profile for soft annealing and sulfurization step.

ious stacking orders like Sn/Zn/Cu, Zn/Sn/Cu, Zn/Cu-Sn, etc. Again, it is difficult to obtain homogenous and compact Cu-Zn-Sn metallic precursors through simultaneous electrodeposition from single electrolyte due to the large reduction potential gaps among the metal ions. For this reason, sequential electrodeposition of Cu-Zn-Sn has been preferred by many researchers.

Several groups attempted to fabricate CZTS thin films over the past few years by electrodeposition-annealing route. In 2008, Scragg et al. first reported sequential electrodeposition of metal precursors in the order Zn/Sn/Cu on Mo/SLG substrate followed by sulfurization at 550 °C for 2 h with 0.8% conversion efficiency [6]. In 2009, Araki et al. reported CZTS thin films from electrodeposited stacked precursors followed by sulfurization at 600 °C which exhibited 0.98% conversion efficiency [7]. Again in 2009, Araki et al. reported CZTS thin films from co-electrodeposited Cu-Zn-Sn precursors followed by sulfurization at 600 °C, showed 3.16% conversion efficiency [8]. In 2009, Ennaoui et al. fabricated CZTS thin films from co-electrodeposited Cu-Zn-Sn precursors followed by sulfurization at 550 °C for 2 h and achieved 3.4% conversion efficiency [9]. In this study, they observed secondary phases such as ZnS in Zn-rich precursor and Cu_2SnS_3 in Zn-poor precursors. In 2010, Scragg et al. reported sequential electrodeposition of Cu/Zn/Sn/Cu on Mo coated SLG precursors followed by sulfurization at 575 °C for 2 h and achieved 3.2% conversion efficiency [10]. In 2012, Ahmed et al. showed substantial growth on conversion efficiency of CZTS thin films solar cells by electrodeposition–annealing approach [11].They have achieved 7.3% conversion efficiency of CZTS from sequential electrodeposition of metallic precursors in the order Cu/Zn/Sn and Cu/Sn/Zn which were followed by sulfurization at 585 °C for 5–15 min. Moreover, they soft-annealed the precursors before sulfurization at temperatures between 210 °C and 350 °C (300 °C was found the best) in order to obtain well mixed and homogenous CuSn and CuZn alloys. As a result, they decreased the sulfurization time from 2 h to 5–15 min with respect to previous studies. In 2013, Lin et al. showed the mechanistic aspects of soft-annealing effects of electrodeposited metallic stacked precursors with 5.6% conversion efficiency [12]. Recently, Jiang et al. demonstrated fabrication of CZTS through electrodeposition-annealing route from stacked metal precursors of Cu-Zn-Sn with 8% power conversion efficiency [13]. This is the highest conversion efficiency of CZTS by electrodeposition-annealing approach to the best of our knowledge. Very recently also an 8.2% efficient pure selenide kesterite (CZTSe) thin film solar cells through electrodeposition-annealing route have been demonstrated by Vauche [14].

In this paper, we propose a CZTS thin-film fabrication process that involves co-electrodeposition of Cu-Sn layer on Mo foil substrate [15] and subsequent Zn electrodeposition on the Cu-Sn/Mo layer from a different solution. This stacking order of Zn/Cu-Sn/Mo has been chosen in order to minimize Sn loss during sulfurization [7,21]. Later, electrodeposited metal stacks were soft-annealed at 350 °C [12] and then sulfurized at 585 °C to obtain well-formed kesterite CZTS.

2. Experimental

Electrodeposition of precursor layers were performed galvanostically in a conventional electrochemical cell assembly at room temperature using an AMEL Potentiostat Model-549. Mo foil substrate (200 μm thick from Goodfellows) with exposed area $1 \times 1\,cm^2$ was used as a working electrode, Titanium mesh was used as a counter inert electrode. The electrolyte for the electrodeposition of Cu-Sn contains 0.026 M Copper-sulfate ($CuSO_4{\cdot}5H_2O$) (Sigma Aldrich); 0.15 M Tin-sulfate ($SnSO_4$) (Fluka), 2 M Methane

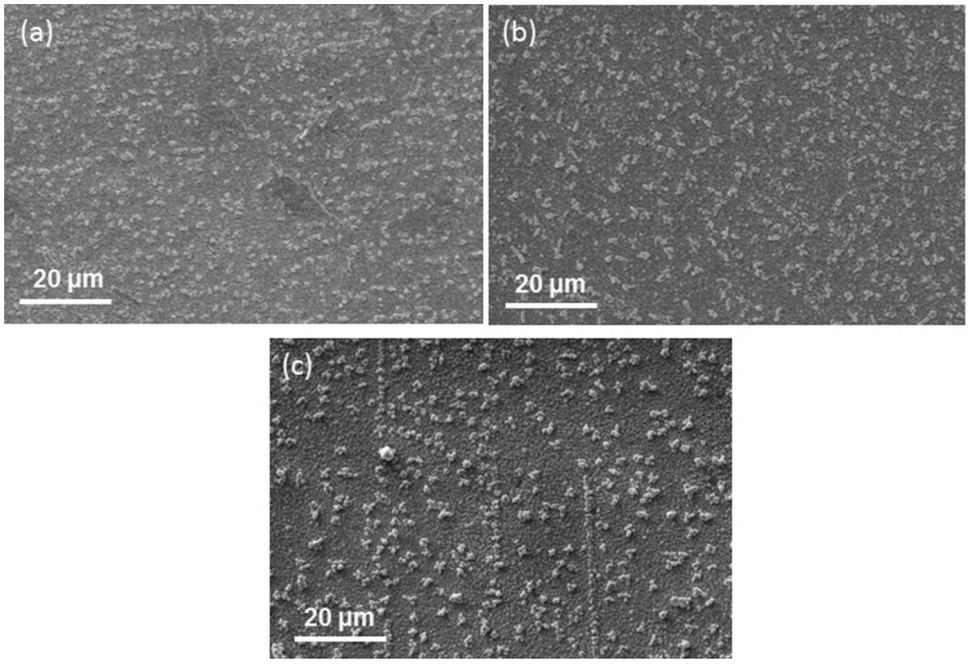

Fig. 2. Surface morphology of as deposited Cu-Sn (a), Zn/Cu-Sn (b) and soft-annealed Zn/Cu-Sn (c) on Mo foil substrate.

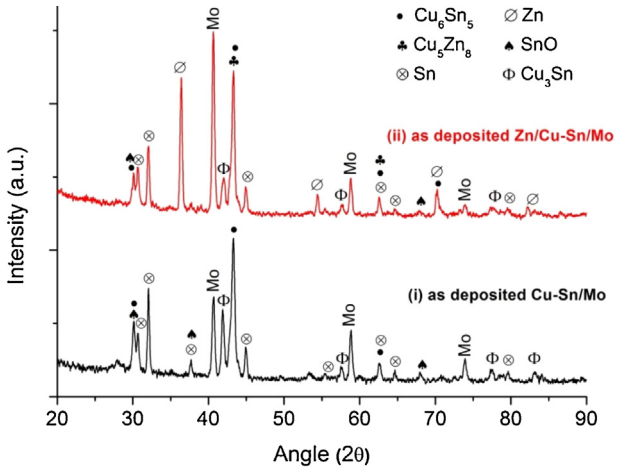

Fig. 3. XRD of (i) as deposited Cu-Sn and (ii) as deposited Zn/Cu-Sn on Mo foil substrate.

sulfonic acid (CH_3SO_3H) (Sigma Aldrich), 0.01 M Hydroquinone ($C_6H_4(OH)_2$) (Carlo Erba Reagents) whereas Zn was electrodeposited from commercial electrolyte bath (Technochimica s.r.l). pH of the Cu-Sn electrolyte and Zn electrolyte were 1.1 and 5.5 respectively. The desired composition of Cu-Sn (Cu:Sn 52:48 wt%; ±2%) was obtained using current density 2.5 mA/cm^2. The desired thickness of the film was 500 nm (±20 nm) and was obtained by setting the time at 10 min. On the other hand, 200 nm Zn layer was deposited on Cu-Sn layer using current density 2 mA/cm^2 with 6 min deposition times. Different Cu-poor, Zn-rich precursors of Cu-Zn-Sn were obtained with the help of different Zn deposition times (5.5 min, 6 min, 6.5 min). At the end of electrodeposition, 650–750 nm Cu-Zn-Sn stacks have been fabricated.

After electroplating, Cu-Zn-Sn precursors were soft annealed at 350 °C with ramping rate 20 °C/min for 20 min in a quartz tube furnace with the presence of very small flow of N_2 (see Fig. 1) [12]. Later soft-annealed Cu-Zn-Sn stacks were sulfurized at 585 °C in 25–30 mg elemental sulfur atmosphere with the same conditions as described in the case of the soft annealing step. A ramping rate of 20 °C/min was chosen according to our previous studies [16].

The crystallographic phase of as deposited Cu-Sn, Cu-Zn-Sn, soft annealed Cu-Zn-Sn and sulfurized films were analyzed by X-ray diffraction (XRD), using a Philips X-pert MPD with CuKα = 1.5406 Å radiation. The surface morphology and the compositional studies of those films were investigated by Scanning Electron Microscopy (Model Zeiss EVO 50) equipped for energy dispersive X-ray spectroscopy (EDS) (Oxford instrument, Model 7060). Here electron energy was set at 20 KeV both for imaging and EDS elemental compositions measurement. Johnson et al. reported recently that with 15 KeV electron energy, EDS probe depth is around 2 μm for CZTS film. So it is assumed here that with 20 KeV electron energy, EDS probe depth will be more than 2 μm and compositions of entire CZTS film will be measured [17]. Raman measurements were carried out in air at room temperature with a Labram HR800Horiba Jobin Yvon micro-Raman spectrometer in backscattering configuration. The spectrometer is equipped with a Peltier cooled CCD and employing two laser sources, a solid-state laser (Laser XTRA, Toptica Photonics) operating at 785 nm, and an argon ion laser (Stabilite 2017, Spectra Physics) operating at 514.5 nm. The laser power density was chosen to generate the best signal to noise ratio in order to avoid sample local heating.Glow discharge optical emission spectroscopy (GDOES) was also carried out by using Spectrum Analytic GmbH (Model GDA 750 analyzer). Photoluminescence (PL) spectra of the films have been studied at 12 K temperature with above bandgap excitation (λexc = 805 nm). All PL measurements were performed with a spectral resolution of 6.6 nm using a standard lock-in technique in conjunction with a single grating monochromator and an InGaAs detector.

Table 1
Metal content and compositional ratios of metal stacks.

Sample No.	Cu (at.%)	Zn (at.%)	Sn (at.%)	Cu/(Zn + Sn)	Zn/Sn	Zn/Cu	Sn/Cu
C55	45.8	27.87	26.33	0.84	1.06	0.60	0.57
C60	41.84	32.53	25.63	0.72	1.27	0.77	0.61
C65	39.16	38.86	21.98	0.64	1.76	0.99	0.56

3. Results and discussions

Due to the high conductivity of Cu and its comparative inert nature during deposition of other metals on it, Cu has been chosen as an under-layer for the fabrication of Kesterites by most of the researchers when stacking order of precursors (Cu-Zn-Sn) are considered [18]. As a result, Zn/Sn layer or Sn/Zn layer are used to deposit on top of Cu. In order to overcome the issues of metal exchange and layer stripping during sequential electrodeposition, Mo/Cu/Sn/Zn sequence has been chosen by almost all researchers for the fabrication of stacked layer precursor for Kesterite. Highest efficient Kesterite based thin film solar cells have been fabricated from this sequence also [18]. It has been observed that the loss of Zn during sulfurization is inevitable as it does not depend whether Zn layer is deposited in the middle or at the top of the stacking layer [19]. Hence more emphasize has been given here to minimize the loss Sn during sulfurization. On the other hand, morphology of Sn is quite porous with respect to other metals which leads to non-homogeneous nucleation of Zn if Zn is deposited on top of Sn. Uniformity of the Zn layer is largely dependent on the uniformity of the underlying Sn layer. As a consequence, in order to overcome all those issues binary Cu-Sn layer has been chosen here as an under-layer. The possibility of Sn loss during sulfurization is also minimized when Sn is co-deposited with Cu in the under-layer.

Fig. 2 shows the SEM images of as deposited Cu-Sn (a), as deposited Zn/Cu-Sn (b) and soft annealed Zn/Cu-Sn (c) on Mo foil substrate, respectively. It can be seen that both the as deposited layers are adherent to the substrate, show dense packaging and homogeneous distribution of grains along the surface. No peeling off has been observed during electrodeposition of Cu-Sn and Zn. After soft-annealing also, Zn/Cu-Sn(c) is found adherent and homogeneous. Furthermore, the morphology of the soft-annealed Cu-Zn-Sn stacks does not show any differences with respect to different elemental ratios of Cu/(Zn + Sn) and Zn/Sn of different samples.

The compositions of as deposited Cu-poor and Zn-rich precursors after soft-annealing, were measured by EDS, as shown in Table 1. Here C55, C60 and C65 samples correspond to 5.5, 6.0 and 6.5 deposition times of Zn on Cu-Sn successively while keeping constant the parameter of Cu-Sn deposition (current density: 2.5 mA/cm^2, deposition time: 10 min).

Fig. 3 shows the XRD spectra of (i) as deposited Cu-Sn and (ii) as deposited Zn/Cu-Sn on Mo foil substrate. XRD pattern of as deposited Cu-Sn/Mo was composed of binary η-Cu_6Sn_5 phase (JCPDS card 47-1575), pure Sn (JCPDS card 86-2264) as well as low intense SnO phase (JCPDS card 01-0902). While XRD pattern of as deposited Zn/Cu-Sn was composed of η-Cu_6Sn_5, γ-Cu_5Zn_8 (JCPDS card 25-1228), pure Zn (JCPDS card 01-1238), pure Sn phases as well as low intensity SnO. Formation of η-Cu_6Sn_5 and γ-Cu_5Zn_8 alloy is reported in both precursors (co-electrodeposited/stacked layer of Cu-Zn-Sn) [20,21].

Fig. 4 shows the XRD spectra of (iii) soft-annealed Cu-Zn-Sn metallic precursors and (iv) sulfurized films (C60). XRD pattern of soft-annealed precursors was composed of Cu_6Sn_5, γ-Cu_5Zn_8 and

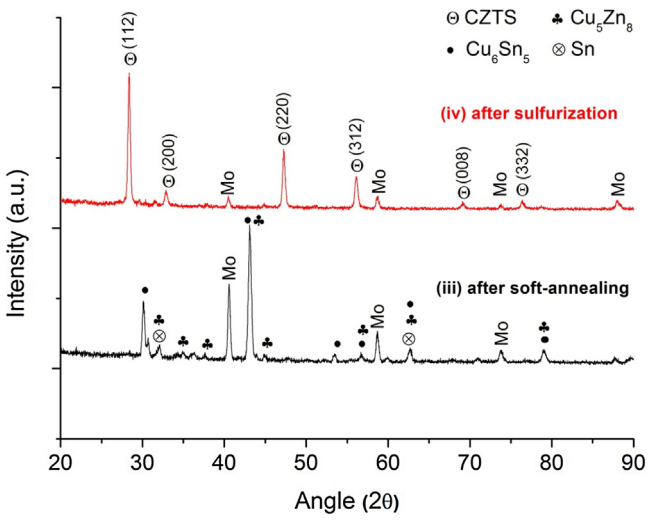

Fig. 4. XRD of (iii) after soft-annealing (C60) and (iv) after sulfurization (C60).

pure Sn. It has been observed that after soft-annealing, pure Zn phase completely disappeared and intensity of pure Sn phases have been reduced. At the same time, the SnO peaks disappeared after soft-annealing, which is in agreement with the literature [22]. As expected, there has been no formation of Zn-Sn phases after electrodeposition of Zn on Cu-Sn layer and soft-annealing step. After sulfurization at 585 °C for 15 min, all the three samples mostly exhibited peaks corresponding to the typical kesterite structure of CZTS in the XRD patterns. Fig. 4(iv) shows the typical polycrystalline kesterite CZTS (JCPDS 26-0575) with dominant peak at diffraction angle $2\Theta = 28.53°$, which has been observed by many others [11,16,21,23]. No secondary phases have been observed after sulfurization in XRD patterns of all samples.

The composition of sulfurized films measured by EDS is reported in Table 2. It should be remarked that the S content is absent since EDS is not able to measure the right quantity of sulfur in the films when Mo is present. In fact, EDS can not resolve sulfur from molybdenum, due to the overlapping energy peak, namely Mo Lα and S Kα [26]. Moreover, Mo signal is also removed from EDS spectrum while measuring the elemental compositions of Cu, Zn and Sn before and after sulfurization. It can be noted that all of CZTS films remain Cu-poor after sulfurization, and the Zn content decreased, due to the volatile effect of Zn during sulfurization [7,24,25,28]. The intensity of Zn loss can be easily understood from the Zn/Cu ratio before and after sulfurization which is demonstrated on Tables 1 and 2. This result is also confirmed by inductively coupled plasma-mass spectrometry (ICP-MS) analysis. A more relevant Zn loss was expected, as the Zn layer was deposited on the top of the metal stack. Loss of Sn (in the form of SnS) during sulfurization has also been reported in many literature works [7,26] which was not observed in our samples. In fact, if we compare the ratios of Sn/Cu before and after sulfurization, any significant loss of Sn is not observed upon sulfurization, which is favourable for CZTS fabrication.

Table 2
Metal content and compositional ratios of sulfurized films.

Sample No.	Cu (at.%)	Zn (at.%)	Sn (at.%)	Cu/(Zn + Sn)	Zn/Sn	Zn/Cu	Sn/Cu
C55	45.74	24.70	29.25	0.85	0.84	0.54	0.63
C60	44.49	28.40	27.10	1.04	1.04	0.63	0.60
C65	43.79	30.40	25.81	0.78	1.17	0.69	0.58

Fig. 5 shows the SEM surface of different sulfurized films: layers are adherent and homogenous morphology in terms of grain size along the films was observed. No substantial differences in morphology of the sulfurized films with respect to various compositional ratios of Cu-Zn-Sn precursors were observed.

Owing to the very similar crystal structure of CZTS and some of its most common secondary phases (e.g. ZnS and Cu_2SnS_3), Raman characterizations are required to demonstrate their presence, as no evidence can be inferred from XRD analyses. Here two excitation wavelengths have been used (i.e. 514.5 and 785 nm) for the characterization of CZTS films. It has been reported earlier by Fernandes et al. that 785 nm radiation penetrates 400 nm, whereas 514.5 nm penetrates 150 nm through CZTS thin films [26]. Raman spectra have been carried out at low laser power density in order to minimize any thermal effect on the sample that can cause struc-

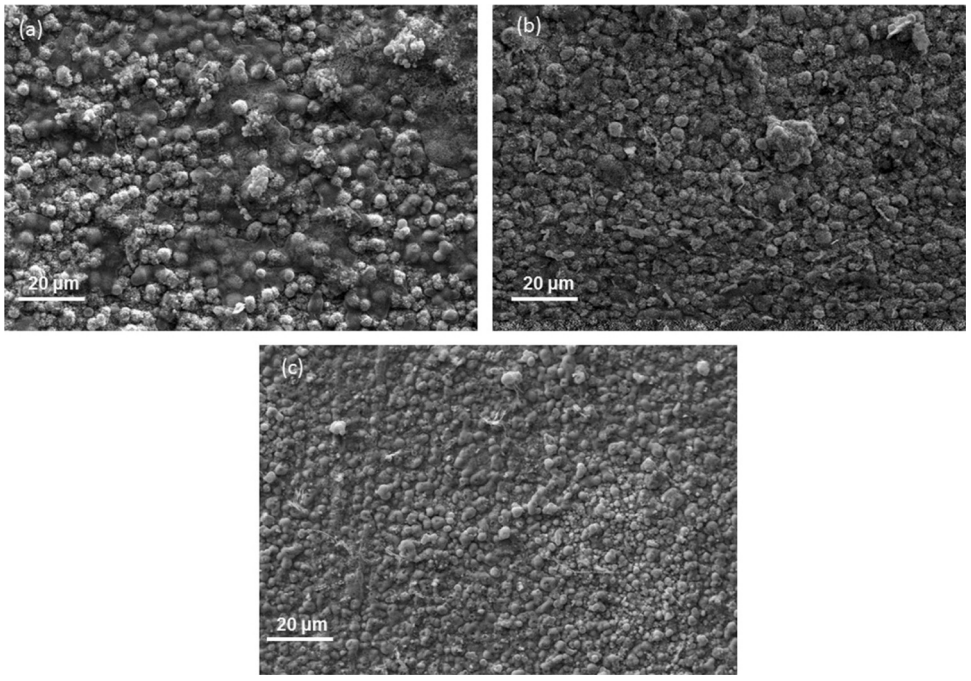

Fig. 5. SEM surface morphology of sulfurized films a (C55), b (C60) and c (C65).

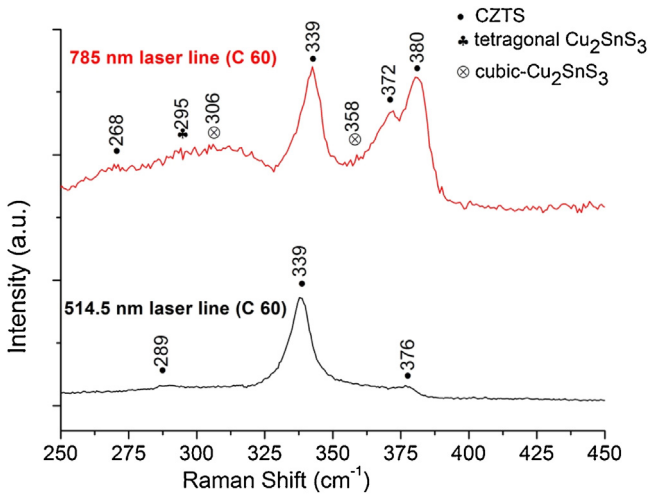

Fig. 6. Comparative Raman spectra of sample (C60) when two different excitation wavelengths are used as laser source.

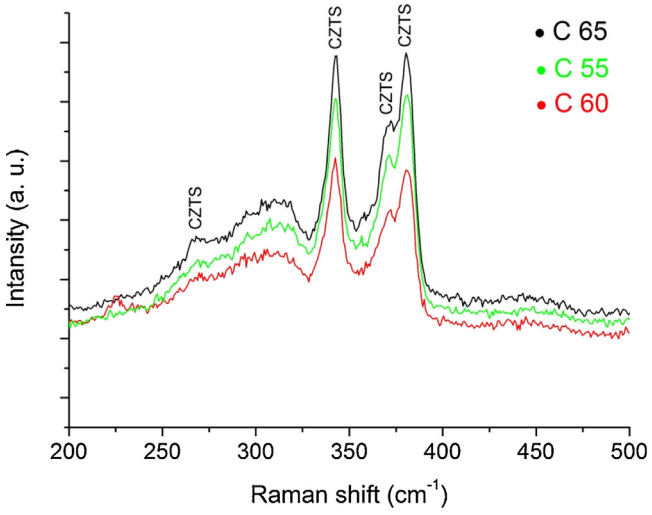

Fig. 7. Raman spectra for three different samples when 785 nm excitation line is used.

tural changes in the films. From Fig. 6, it is visible that 514.5 nm excitation line shows typical Raman peaks at 289 cm^{-1}, 339 cm^{-1} and 376 cm^{-1} related to Kesterite-CZTS phase without any secondary phases, which is in good agreement with the results of previous studies [11,12,16,26] with a commonly acknowledged highest intensity peak at 337–339 cm^{-1} for CZTS. Conversely, with 785 nm excitation line new broad and weak bands at 295 cm^{-1}, 306 cm^{-1} and 358 cm^{-1} are observed. These bands can be possibly attributed to secondary phases like tetragonal Cu_2SnS_3 (295 cm^{-1}) and cubic Cu_2SnS_3 (306 cm^{-1}, 358 cm^{-1}) based on the previous studies [26,29]. It should be noted that with 785 nm laser line the CZTS Raman peaks at 268 cm^{-1}, 372 cm^{-1} and 380 cm^{-1} have been observed whereas they did not appear with 514.5 nm excitation wavelengths, as previously observed in the literature [26].This effect has been attributed to different penetration depths of 785 nm (400 nm) and 514.5 nm (150 nm) laser lines. Change of relative intensity in CZTS Raman peaks observed with 785 and 514.5 nm excitation lines may be attributed to different resonance conditions [26].

Fig. 7 shows a comparison between the Raman spectra of three different samples using the 785 nm excitation wavelength. It is visible from the figure that sample C 60 has less intense secondary

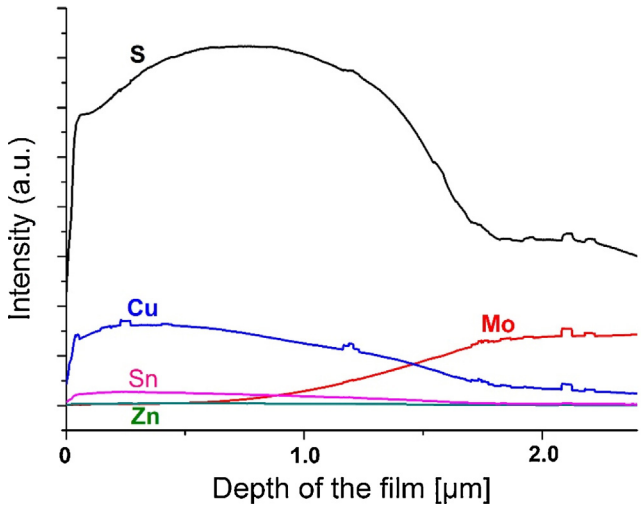

Fig. 8. GDOES profile of sulfurized film (C60).

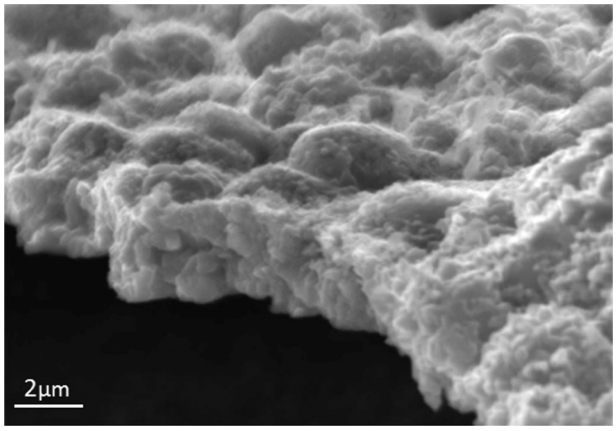

Fig. 9. SEM Cross-sectional view of sulfurized film (C60).

phases with respect to other two. So from this point of view, precursor composition (Cu: 41.84, Zn: 32.53 and Sn: 25.63) is the best among the three samples.

Sample C 60 was further characterized by GDOES to investigate the distribution of elements along the film thickness. It is clear from Fig. 8 that composition of CZTS film does not change that much along the film thickness in case of sample C 60. What is interesting in GDOES profile of sulfurized film is that there is no evidence of ZnS segregation at the interface of CZTS/Mo, as Zn intensity does not show any upward trend in that region unlike [19]. Segregation of ZnS used to be reported in other literatures [9,27,30]. As there is no sign of formation of ZnS at the CZTS/Mo interface and concentration of Cu decrease along the depth in GDOES profile, formation of solid SnS_2 (even if Sn concentration is not increased at that region) can be proposed to this phenomenon. On the other hand, the increase of Mo signal is not sharp at the CZTS/Mo interface in GDOES profile. The formation of MoS_2 can not be claimed conclusively on that region as non-uniform CZTS film thickness can also be reason behind that unsharp Mo signal [27]. Further investigations are needed in order to fully understand those phenomenon.

Fig. 9 shows the cross-section image of sulfurized CZTS film: the thickness of CZTS film is around 2 μm. It also shows that film is somewhat rough. As a result, CZTS film has been characterized by laser profilometer and roughness was found in the range of 200–300 nm. Roughness of the film can be reduced by performing prolong soft-annealing treatment on precursor before sulfurization [12] which is under investigation at the moment.

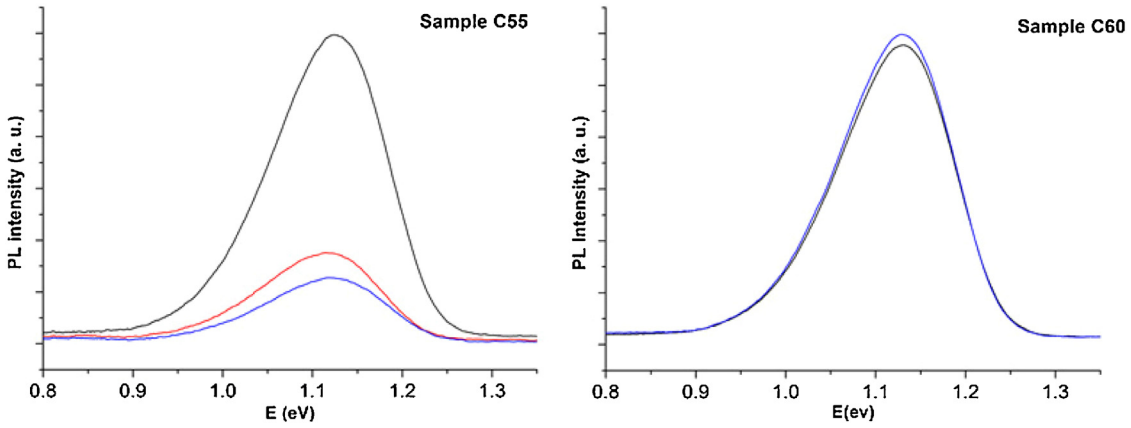

Fig. 10. Photoluminescence (PL) spectra of samples (C55) and (C60) at 15 K ($\Delta\lambda = 6.6$ nm, $P = 6$ W/cm^2).

In order to investigate the possible presence of levels in the bandgap detrimental for both for optoelectronic and photovoltaic applications, some of the samples (C55, C60) were characterized by PL spectroscopy at low temperature (15 K). According to many literature works, broad PL bands are observed between 1 and 1.3 eV in CZTS layers [31–34] at low temperature. In our studies, a broad peak appears in both samples at around 1.15 eV (Fig. 10), which was recently reported in [33]. According to [33], this peak shows power and temperature dependence typical of radiative recombinations known as quasi-donor-acceptor pair (QDAP) transitions, which involve potential fluctuations [34].This behavior is well known in highly defective and compensated semiconductors [35], where inversely charged defects and fluctuations in the defect concentration lead to irregular fluctuations of the electrostatic potential with position. This random defect potential perturbs the band states energies and induces a modification of the well-defined energy levels into broad band states. Consequently, localized shallow levels associated to charged defects lose their original discrete characteristics and merge with the valence and conduction bands. In case of sample C55, relative intensity of individual peaks (different colour in graph) were observed in different regions of sample whereas in case of sample C60, no variation of individual peaks were observed with respect to different regions. This behaviour can be attributed to the spatial variation in the CZTS film [33]. According to Gershon et al. [35], CZTS layers whose PL spectrum consists of a QDAP emission with saturated peak energy position towards 1.18 eV are very efficient PV absorbers.

4. Conclusions

CZTS has been successfully fabricated through electrodeposition-annealing route from electrodeposited stacked bilayer precursor (Zn/Cu-Sn/Mo). Metal stacks were adherent to the substrate with homogeneous morphology. Though Zn losses have been observed upon sulfurization, no Sn losses were noticed, which is probably connected to the stacking order of precursors. Raman spectra recorded with 785 nm laser line showed more secondary phases with respect to those observed with the 514.5 nm excitation line. This effect is probably due to a different penetration depth in the case of 785 and 514.5 nm excitations respectively. Photoluminescence results reveal the suitability of the film as an absorber layer for thin film solar cells.

References

[1] Photovoltaics Report, Fraunhofer Institute for solar energy systems ISE, 24 October, 2014.
[2] K. Ito, T. Nakazawa, Electrical and optical properties of stannite-type quaternary semiconductor thin films, Jpn. J. Appl. Phys. 27 (1988) 2094–2097.
[3] W. Shockley, H.J. Queisser, Detailed balance limit of efficiency of p-n junction solar cells, J. App. Phys. 32 (1961) 510.
[4] W. Wang, M.T. Winkler, O. Gunawan, T. Gokmen, T.K. Todorov, Y. Zhu, D.B. Mitzi, device characteristics of CZTSSe thin-film solar cells with 12.6% efficiency, Adv. Energy Mater. 4 (2014) 1301465.
[5] T. Kato, H. Hiroi, N. Sakai, S. Muraoka, H. Sugimoto, Characterization of front and back interfaces of Cu_2ZnSnS_4 thin-film solar cells, 27th EU PVSEC (2012), http://dx.doi.org/10.4229/27thEUPVSEC2012-3CO.4.2.
[6] J.J. Scragg, P.J. Dale, L.M. Peter, G. Zoppi, I. Forbes, New routes to sustainable photovoltaics: evaluation of Cu_2ZnSnS_4 as an alternative absorber material, Phys. Status Solidi B 245 (2008) 1772–1778.
[7] H. Araki, Y. Kubo, A. Mikaduki, K. Jimbo, W.S. Maw, H. Katagiri, M. Yamazaki, K. Oishi, A. Takeuchi, Preparation of Cu_2ZnSnS_4 thin films by sulfurizing electroplated precursors, Sol. Energy Mater. Sol. Cells 93 (2009) 996–999.
[8] H. Araki, Y. Kubo, K. Jimbo, W.S. Maw, H. Katagiri, M. Yamazaki, K. Oishi, A. Takeuchi, Preparation of Cu_2ZnSnS_4 thin films by sulfurization of co-electroplated Cu-Zn-Sn precursors, Phys. Status Solidi C 6 (2009) 1266–1268.
[9] A. Ennaoui, M. Lux-Steiner, A. Weber, D. Abou-Ras, I. Kotschau, H.-W. Schock, R. Schurr, A.H. olzing, S. Jost, R. Hock, T. Voß, J. Schulze, A. Kirbs, Cu_2ZnSnS_4 thin film solar cells from electroplated precursors: novel low-cost perspective, Thin Solid Films 517 (2009) 2511–2514.
[10] J.J. Scragg, D.M. Berg, P.J. Dale, A 3.2% efficient kesterite device from electrodeposited stacked elemental layers, J. Electroanal. Chem. 646 (2010) 52–59.
[11] S. Ahmed, K.B. Reuter, O. Gunawan, L. Gao, L.T. Romankiw, H. Deligianni, A high efficiency electrodeposited Cu_2ZnSnS_4 solar cell, Adv. Energy Mater. 2 (2012) 253–259.
[12] Y. Lin, S. Ikeda, W. Septina, Y. Kawasaki, T. Harada, M. Matsumura, Mechanistic aspects of preheating effects of electrodeposited metallic precursors on structural and photovoltaic properties of Cu_2ZnSnS_4 thin films, Sol. Energy Mater. Sol. Cells 120 (2014) 218–225.
[13] F. Jiang, S. Ikeda, T. Harada, M. Matsumura, Pure sulfide Cu_2ZnSnS_4 thin film solar cells fabricated by preheating an electrodeposited metallic stack, Adv. Energy Mater. 4 (2014) 1301381.
[14] L. Vauche, Y. Risch, M. Sánchez, M. Dimitrievska, T. Pasquinelli, P. Goislard de Monsabert, S. Grand, E. Jaime-Ferrer, 8.2% pure selenide kesterite thin-film solar cells from large-area electrodeposited precursors, Prog. Photovolt.: Res. Appl. (2016), http://dx.doi.org/10.1002/pip.2643.
[15] C.T.J. Low, F.C. Walsh, Electrodeposition of tin, copper and tin–copper alloys from a methane sulfonic acid electrolyte containing a perfluorinated cationic surfactant, Surf. Coat. Technol. 202 (2008) 1339–1349.
[16] M.I. Khalil, R. Bernasconi, L. Magagnin, CZTS layers for solar cells by an electrodeposition-annealing route, Electrochim. Acta 145 (2014) 154–158.
[17] M.C. Johnson, C. Wrasman, X. Zhang, M. Manno, C. Leighton, E.S. Aydil, Self-regulation of Cu/Sn ratio in the synthesis of Cu_2ZnSnS_4 films, Chem. Mater. 27 (2015) 2507–2514.
[18] D. Colombara, A. Crossay, L. Vauche, S. Jaime, M. Arasimowicz, P.P. Grand, P.J. Dale, Electrodeposition of kesterite thin films for photovoltaic applications: quo vadis? Phys. Status Solidi A 212 (2015) 88–102.
[19] L. Vauche, J. Dubois, A. Laparre, M. Pasquinelli, S. Bodnar, P. Grand, S. Jaime, Rapid thermal processing annealing challenges for large scale Cu_2ZnSnS_4 thin films, Phys. Status Solidi A 212 (2014) 103–108.
[20] J.J. Scragg, Studies of Cu_2ZnSnS_4 Films Prepared by Sulfurisation of Electrodeposited Precursors, PhD Thesis, University of Bath, 2010.
[21] K.V. Gurav, S.M. Pawar, S.W. Shin, M.P. Suryawanshi, G.L. Agawane, P.S. Patil, J.H. Moon, J.H. Yun, J.H. Kim, Electrosynthesis of CZTS films by sulfurization of CZT precursor: effect of soft annealing treatment, Appl. Surf. Sci. 283 (2013) 74–80.

[22] R. Kondrotas, R. Juskenas, A. Naujokaitis, A. Selskis, R. Giraitis, Z. Mockus, S. Kanapeckaite, G. Niaura, H. Xie, Y. Sanchez, E. Saucedo, Characterization of $Cu_2ZnSnSe_4$ solar cells prepared from electrochemically co-deposited Cu-Zn-Sn alloy, Sol. Energy Mater. Sol. Cells 132 (2015) 21–28.
[23] S. Marchionna, P. Garattini, A. Le Donne, M. Acciarri, S. Tombolato, S. Binetti, Cu_2ZnSnS_4 solar cells grown by sulphurisation of sputtered metal precursors, Thin Solid Films 542 (2013) 114–118.
[24] P.A. Fernandes, P.M.P. Salome, A.F. da Cunha, Growth and Raman scattering characterization of Cu_2ZnSnS_4 thin films, Thin Solid Films 517 (2009) 2519–2523.
[25] J.J. Scragg, T. Ericson, T. Kubart, M. Edoff, C. Platzer-Bjorkman, Chemical Insights into the instability of Cu_2ZnSnS_4 films during annealing, Chem. Mater. 23 (2011) 4625–4633.
[26] P.A. Fernandes, P.M.P. Salome, A.F. da Cunha, Study of polycrystalline Cu_2ZnSnS_4 films by Raman scattering, J. Alloys Compd. 509 (2001) 7600–7606.
[27] C. Platzer-Björkman, J. Scragg, H. Flammersberger, T. Kubart, M. Edoff, Influence of precursor sulfur content on film formation and compositional changes in Cu_2ZnSnS_4 films and solar cells, Sol. Energy Mater. Sol. Cells 98 (2012) 110–117.
[28] M.I. Khalil, R. Bernasconi, S. Ieffa, A. Lucotti, S. Binetti, A. Le Donne, L. Magagnin, Effect of co-electrodeposited Cu-Zn-Sn precursor compositions on the final sulfurized CZTS thin films for solar cell, ECS Trans. 64 (2015) 33–41.
[29] M. Altosaar, J. Raudoja, K. Timmo, M. Danilson, M. Grossberg, J. Krustok, E. Mellikov, $Cu_2Zn_{1-x}Cd_xSn(Se_{1-y}S_y)_4$ solid solutions as absorber materials for solar cells Phys, Status Solidi A 205 (2008) 167–170.
[30] R.B.V. Chalapathy, G.S. Jung, B.T. Ahn, Fabrication of Cu_2ZnSnS_4 films by sulfurization of Cu/ZnSn/Cu precursor layers in sulfur atmosphere for solar cells, Sol. Energy Mater. Sol. Cells 95 (2011) 3216–3221.
[31] S. Siebentritt, S. Schorr, Kesterites—a challenging material for solar cells, Prog. Photovolt.: Res. Appl. 20 (2012) 512–519.
[32] K. Tanaka, T. Shinji, H. Uchiki, Photoluminescence from Cu_2ZnSnS_4 thin films with different compositions fabricated by a sputtering-sulfurization method, Sol. Energy Mater. Sol. Cells 126 (2014) 143–148.
[33] L. Van Puyvelde, J. Lauwaert, P.F. Smet, S. Khelifi, T. Ericson, J.J. Scragg, D. Poelman, R. Van Deun, C. Platzer-Björkman, H. Vrielinck, Photoluminescence investigation of Cu_2ZnSnS_4 thin film solar cells, Thin Solid Films 582 (2015) 146–150.
[34] S. Le Donne, P. Marchionna, R.A. Mereu, M. Acciarri, S. Binetti, Effects of CdS buffer layers on photoluminescence properties of Cu_2ZnSnS_4 solar cells, Int. J. Photoenergy (2015) 583058.
[35] T. Gershon, B. Shin, T. Gokmen, S. Lu, N. Bojarczuk, S. Guha, Relationship between Cu_2ZnSnS_4 quasi donor-acceptor pair density and solar cell efficiency, Appl. Phys. Lett. 103 (2013) 193903.